JTTEE5 16:261–274
DOI: 10.1007/s11666-007-9024-9
1059-9630/$19.00 © ASM International

Plasma Spray Deposition on Inclined Substrates: Simulations and Experiments

C.W. Kang, H.W. Ng, and S.C.M. Yu

(Submitted March 1, 2006; in revised form June 13, 2006)

In the plasma spray coating process, the coating's profile and overall thickness are dependent on the number of overlapping traverses of the torch, the shape of the particle spray plume, the spatial distribution of the in-flight parameters of the particles within, and the orientation of the substrate. In this paper, a semi-empirical methodology for predicting three-dimensional deposits by the plasma spray process is developed. It comprises of three stages: first, spatial distributions of the in-flight parameters of multi-sized particles within the spray plume are determined by Computational Fluid Dynamics simulations. The size and shape parameters of the splats formed when individual droplets impact and spread out are obtained by experiments. Finally, a computer program is developed to integrate the particle parameters distribution and the empirical splat geometric data to generate a three-dimensional profile representing the deposit. The procedures predict the deposition volumes and thicknesses for different substrate inclinations with good agreement to experimentally sprayed deposits.

Keywords thermal spray, simulation, deposit, substrate inclination

1. Introduction

Plasma spraying is a process by which coatings are applied to surfaces to protect from wear, high temperature, and corrosion. In this process, a plasma source produces high-temperature plasma capable of melting particulate materials including metals and ceramics. The materials are fed into the plasma plume to be melted into droplets that eject at high velocity to impact onto the part to be sprayed. On impact, the droplets form splats that rapidly solidify and adhere onto the surface thus forming a deposit or coating after successive overlap and accumulation of multiple splats.

Many industries have been using plasma spraying for coating engineering components, some of which have complex three-dimensional shapes. For example, internal and external surfaces of oil and gas pipelines are plasma sprayed with coatings to protect against corrosion and chemical attack (Ref 1-3). The hard wearing plasma-sprayed ceramic coatings are also applied on brake discs and combustion engine cylinder bores that are exposed to extreme temperature changes (Ref 4 and 5). Finally in the power generation and aerospace industries, gas turbines blades and combustion chambers are coated with plasma-sprayed ceramic thermal barrier coatings in order to increase the overall thermal efficiency by increasing the gas exit temperature (Ref 6).

However, due to the lack of a predictive model on coating formation on various surface topologies, some of these industries currently spray based on experimental tests and by experience. This technique is frequently time consuming and expensive (e.g., equipment, parts, powders, and gases) and requires highly trained and well-paid operators. For the more safety critical applications, such as gas turbines blades and hot section components, industries have developed in-house smart technologies to control the spraying process. Turbine blades besides having a complex shape are subject to specific requirements on coating thickness, i.e., thicker at the leading edge and reducing toward the trailing edge, hence are more difficult and

C.W. Kang, Institute of High Performance Computing, 1 Science Park Road, #01-01, The Capricorn, Singapore Science Park II, Singapore, 117528, Singapore; **H.W. Ng** and **S.C.M. Yu,** School of Mechanical and Aerospace Engineering, Nanyang Technological University, 50, Nanyang Avenue, Singapore, 639798, Singapore. Contact e-mail: mhwng@ntu.edu.sg.

Nomenclature

D_p	particle diameter (m)
d	splat diameter (m)
d_e	equivalent splat diameter (m)
d_x	minor splat diameter (m)
d_y	major splat diameter (m)
Ra	mean arithmetic surface roughness (m)
r	root locus of ellipse
T_p	particle temperature (K)
t	splat thickness (m)
u_p	particle velocity (m/s)
V_p	particle volume (m^3)
V_s	splat volume (m^3)

Greek symbols

ξ	spread factor: $\xi = d_e/D_p$
ψ	aspect ratio: $\psi = d_y/d_x$
θ	substrate inclination angle (°)

challenging to spray. Therefore, a deposition model of predicting the coating profiles for such parts would be useful in reducing the extent of experimental spraying especially for the first time or ''first cut'' spraying of a new engineering parts or components that have complex shapes. The model can be further developed to compute the path taken by a robotically controlled spray torch to spray a complete turbine blade to the required coating thickness profile.

Recently, Trifa et al. (Ref 7 and 8) presented Gaussian relationships between the processing parameters of atmospheric plasma spray (APS) and the deposit shapes. In their study, the deposits were sprayed under different processing parameters namely: standoff distance, spray angle, spray time, and the angular positioning of the powder injection and later measured by a laser-based measurement system. The net deposit profiles were extracted and then fitted by Gaussian approximations. These Gaussian relationships were used in defining the geometry of a deposit which could be utilized for optimization of robotic trajectories in APS. In this study, a totally different approach has been attempted. A deposition prediction model, combining Computational Fluid Dynamics (CFD) simulation and empirical testing at the splat level is developed to forecast the coating profiles on substrates at different inclination angles. The former part consists of CFD numerical model to solve the single-phase gas temperature and velocity behavior in the plasma plume. The dynamic and thermal behavior of the particles are obtained by the gas to particle momentum and heat transfer coupling models, respectively. The in-flight droplet parameters consisting of sizes, temperatures, velocities, trajectories and hence the impact sites of individual particles inside a spray cone onto the substrate plane are calculated and data stored.

The empirical part of the approach makes use of the splat measurement experiments whereby single splats generated by impact of spray droplets are collected and their dimensions are measured and stored. The database of the likely shape, thickness, and size of splats resulting from impacting droplets of known size and angles of impact is utilized to relate the incoming droplet distributions predicted by the CFD to produce the splats of known dimensions.

The final step performed by the Substrate Cell Model (SCM) involves the integration or reconstruction of the deposit build-up of individual splats. The multiple process simulation steps coupled with intermediate step of empirical calibration can be described as a concept of ''desktop manufacturing.'' The flowchart for the solution procedure is shown in Fig. 1. In future, deposition on surface topography with continuously varying curvature representing realistic engineering artifacts will be implemented by characterizing the curved surface geometry as locally flat facets, each facet having individual inclination.

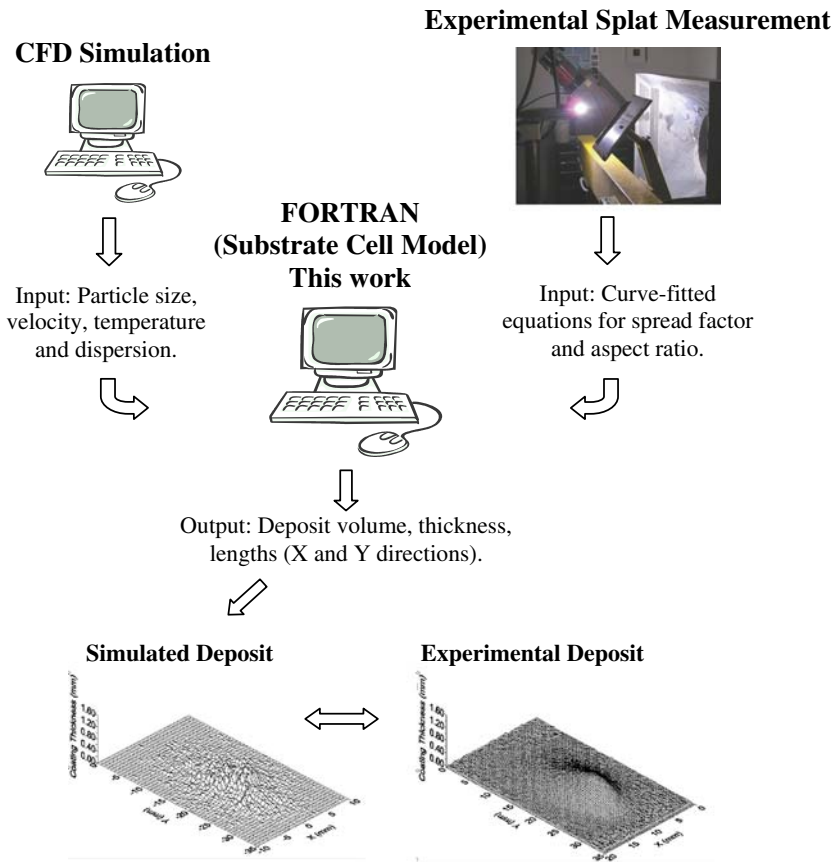

Fig. 1 Flow chart of solution procedure

This paper describes the methodology of the SCM for deposition at different substrate inclinations. The results for simulated deposits from 0° to 60° at 10° intervals of substrate inclinations are presented and compared with test sprayed deposits. The deposition experiment procedure is described and comparison between the computation and experimental deposits shows fairly good agreement.

2. Computational Fluid Dynamics Simulation

Coating formation is the final stage in plasma spraying process. In the modeling of coating formation, in-flight particle behavior, namely: particle size, intensity or number of particle per unit area, temperature, velocity and dispersion are required. The detailed modeling procedures of CFD simulation and assumptions specific to this paper, including the derivation of particle in-flight behavior and spatial dispersion characteristic were previously described by Remesh et al. (Ref 9). Also CFD analyses were routinely carried out by others such as Delplanque and Rangel (Ref 10), Liu et al. (Ref 11), Zhang et al. (Ref 12), and Chang and Ramshaw(Ref 13), the last mentioned being notable as one of the earliest pioneers.

The CFD simulation code used is FLUENT V6.02© commercial package (Fluent Inc., 10 Cavendish Court, Lebanon, NH03766-1442). The finite volume mesh for the model included the torch and the free space in front of the torch for the spray plume. A steady-state thermal fluid solution for the plasma jet comprising of velocity and temperature fields was firstly obtained. The particle dynamics and temperature were calculated from the drag force and convective thermal energy heat transfer models, respectively. During the particle in-flight transition through the plasma jet, it received heat energy raising its temperature to melting point as well as increased its velocity through momentum exchange with the plasma gas. The relationship between particle in-flight velocity, temperature, and size also depended much on the process parameters such as direct current (DC), voltage, gas and particle properties and many others. The exact temperature and velocity of each particle were also depended on its size (diameter) and its path through the plasma plume.

The contour distributions of particles in-flight parameters in terms of diameter, number of particles (concentration), temperature, and velocity are given in Fig. 2. On the left-hand side of the figure, the distributions are obtained for a vertically held substrate (inclined at 0°) while the right-hand side shows the distributions for a substrate inclined at 60° to the vertical. The distributions of particle size and number density will be utilized as the input data for the SCM. The particle number density determines the number of particles arriving at a particular spot on the substrate. The particle diameter distribution is used to calculate the eventual size of the splats via the experimentally derived spread factor.

3. Experimental Splat Measurements

In the literature search on splating mechanisms, it is found that considerable efforts have been devoted to numerical analyses and experimental investigations on the deformation of single liquid droplet impacting onto a flat substrate. Trapaga and Szekely (Ref 14), Feng et al. (Ref 15), Zhang et al. (Ref 16), Pasandideh-Fard et al. (Ref 17), and Mostaghimi et al. (Ref 18) addressed the effect of substrate temperature, solidification, surface tension, and thermal contact resistance on the spreading of single droplet impacting perpendicularly upon the substrate. The deformation and interaction behavior of multiple droplets during impingement onto flat perpendicular substrate were investigated by Liu et al. (Ref 19). Their numerical results showed ejection, rebounding and breakup during the interaction of the droplets. They suggested that these phenomena might reduce the deposition rate and deteriorate the bonding and deposit integrity. In the case of oblique impact, Bussmann et al. (Ref 20) simulated single droplet impacting on an inclined substrate to predict the elongation of the splat. For multiple splats overlapping to form a deposit, Ghafouri-Azar et al. (Ref 21) developed a three-dimensional stochastic deposition model where the particle parameters and impact points were assigned random values along normal distributions. Specific splat models or experimental work related to the yttria-stabilized zirconia material are not available from the literature despite intensive search.

Experiments were carried out to capture individual splats deposited by droplets impacting on a substrate which was the prelude to the current work. A very detailed description of the experimental procedures and measurement techniques was provided in Kang and Ng (Ref 22). The paper had focused on the measurement of splat shape and identifying their morphologies which included well-formed and malformed splats obtained for a range of impact angles. Results of studying over 50 splats of various sizes were condensed into polynomial equations which characterized the spread factor and aspect ratio for various angles of impact. The experiments are briefly described below.

In all the experiments, the powder feedstock was yttria-partially-stabilized (8%) zirconia with size distribution of 22-125 μm (Product code: 204NS) supplied by Saint-Gobain Norton K.K., Singapore and the substrate was mild steel plate. The overlapping and coincident splats were minimized and individual splats were later identified on the substrate and their thicknesses and lengths were measured by means of a high-resolution WYKO NT-2000 optical surface profiler (Veeco Tucson Inc., 2650, East Elvira Road, Tucson, AZ 85706). Some examples of the splats thus isolated are shown in Fig. 3 for angles of inclination of the substrates at 0°, 30° and 60°. From the thickness and area of the splat, it was also possible to calculate its volume and thus deduce the diameter of the originating droplet by means of the principle of volume conservation.

The spread factor parameter determines the diameter of the circular splat given the diameter of the droplet in

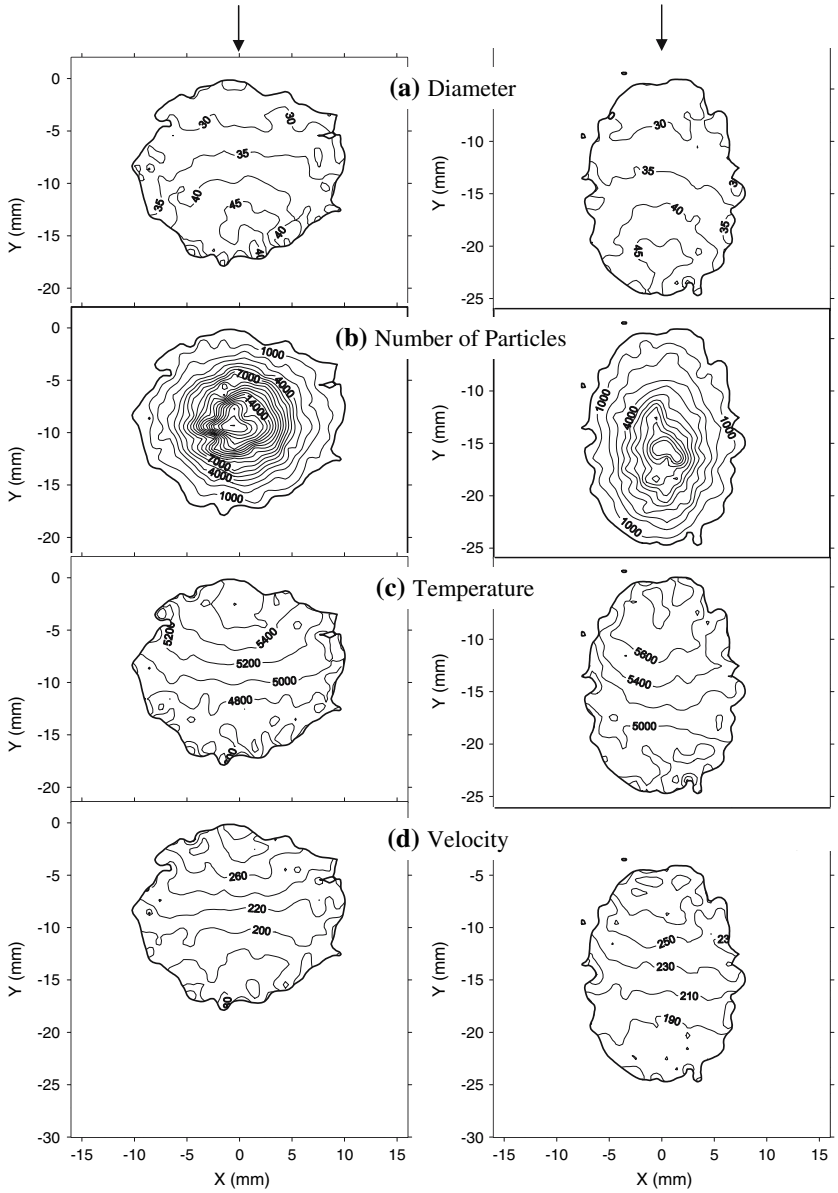

Fig. 2 Contours of computed particle in-flight parameters: (a) diameter (microns), (b) number of particles (n_p), (c) surface temperature (K), and (d) velocity (m/s) for 0° (left) and 60° (right) substrate inclination angles. At top of the figures, arrows show direction of particle injection at torch

the case of perpendicular impact. When spraying a part with complex geometry it is often complicated by off-normal spray angle, which causes spray particles to impact on the substrate obliquely. As the droplet strikes the substrate at an oblique angle, an elliptical shaped splat results and the aspect ratio parameter characterizes the shape of that elliptical splat, by the ratio of the major to minor diameters of the ellipse.

The spread factor, ξ, is defined as the ratio of equivalent splat diameter to droplet diameter, i.e.

$$\xi = \frac{d_e}{D_p} \qquad \text{(Eq 1)}$$

while the aspect ratio, ψ is defined as,

$$\psi = \frac{d_y}{d_x} \qquad \text{(Eq 2)}$$

Both spread factors and aspect ratios were extracted from measurements of the 50 individual splats at each inclination angle θ and the results are shown in Fig. 4 and 5. The polynomial curves, Eq 3 and 4 were best-fitted over the values of spread factor (ξ) and aspect ratio (ψ):

$$\xi = -0.0009\theta^2 + 0.0557\theta + 4.6024[R^2 = 0.9447] \qquad \text{(Eq 3)}$$

$$\psi = 0.0003\theta^2 - 0.0062\theta + 1.0252[R^2 = 0.9823] \qquad \text{(Eq 4)}$$

where θ is the inclination angle. Referring to Eq 3 and 4, the inclination angle is the only independent variable. This

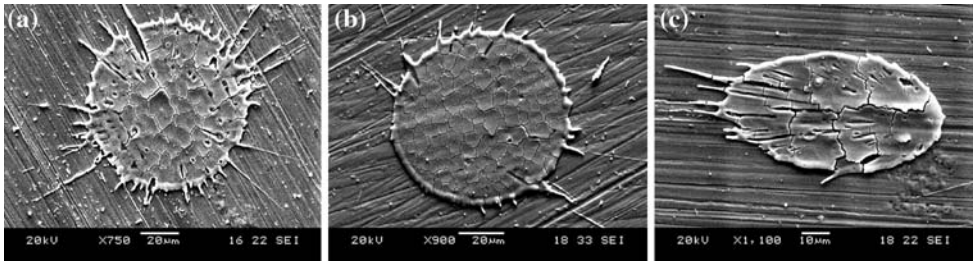

Fig. 3 Some examples of splat obtained from particle impacting at (a) 0°, (b) 30°, and (c) 60° substrate inclinations

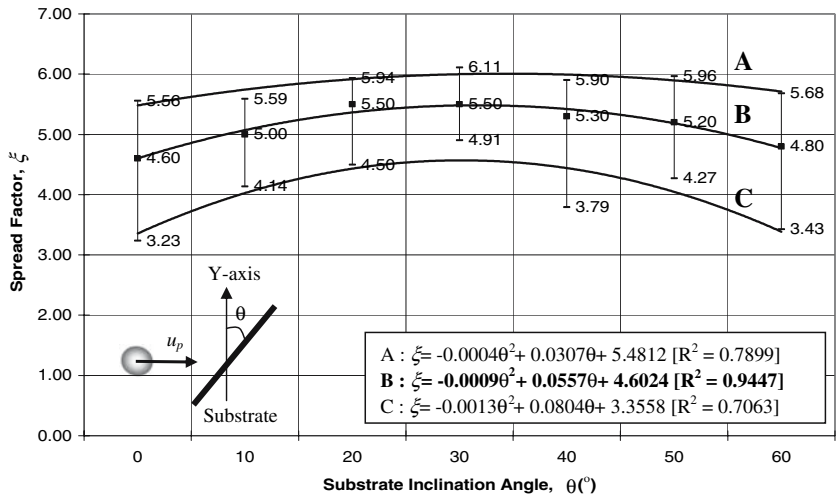

Fig. 4 Experimental spread factors, ξ against substrate inclination angles, curve fitted by quadratic function. Measurement at each inclination is based on 50 splats

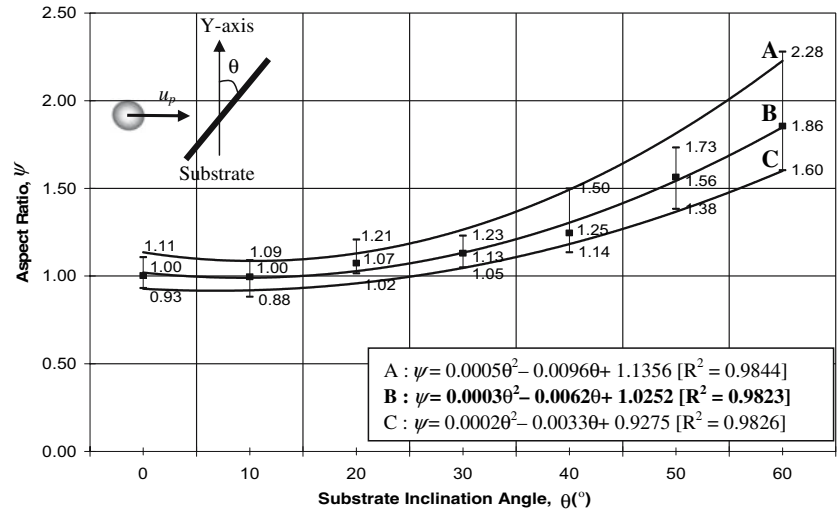

Fig. 5 Plot of aspect ratios, ψ against substrate inclination angles with curve fitted quadratic equation. Fifty (50) splats per inclination are measured

implies that at any inclination angle, both geometric parameters will reduce to a constant, irrespective to particle behavior. In order to have a more comprehensive model, the effect of particle behavior should also be included. Due to the experimental difficulties of measuring the size, temperature, and velocity of each particle just before impact, experimental data on particle in-flight behavior at various inclination angles are currently not

Table 1 Spread factors, ξ obtained by atmospheric plasma-sprayed zirconia on various substrates at different spraying conditions based upon the published data

Author	Process condition	Substrate material	Surface roughness, Ra, μm	Spread factor, ξ
Kang and Ng (Ref 22)	900 A, 35 V, 72 l/min Ar	Polished mild steel	0.50	4.62[a] (3.23-5.56)
Leger et al. (Ref 23)	600 A, 73 V, 43 l/min Ar, 15 l/min H_2	Steel coated with zirconia	0.20 or 4.00	4.70[a]
	600 A, 73 V, 43 l/min Ar, 15 l/min H_2	Steel	0.05, 0.40, or 9.00	4.90[a]
Vardelle et al. (Ref 24)	500 A, 54 V, 36 l/min Ar, 11 l/min H_2	Polished stainless steel	0.10	(3.50-5.50)
Kucuk et al. (Ref 25)	600 A, 63 V, 45 l/min Ar, 11 l/min H_2	Glass microscope slide	0.02	5.50[a] (4.80-6.20)

[a] Note: Average spread factors, ξ from experiments. Bracketed values indicate experimental ranges.

available. However, the authors strongly believe that Eq 3 and 4 are sufficient to be utilized in the coating formation modeling.

In addition, it is noted that the empirical data gathered are very specific and do not include salient parameters related to the process conditions, but it is believed the data can be adopted for the coating formation modeling. As seen in Table 1, the spread factors for zirconia sprayed at different process parameters on a range of substrate materials (glass, stainless steel, and steel coated with zirconia) and with different surface roughness (Ra values range from 0.02 to 9 μm) differ. When considered together with the experimental scatter present, the percentage difference of 10% is tolerable for the coating formation modeling.

4. Substrate Cell Model

The SCM is a FORTRAN© program which processes all the particle parameters and spatial dispersion characteristic to predict the resulting coating profiles for different substrate inclinations.

The substrate of dimensions 35 mm × 20 mm was numerically subdivided into a matrix of square cells of microscopic, i.e., micron dimensions. From grid sensitivity study, discretization of substrate into 8 μm × 8 μm cells was found to be optimum, with a residual error of less than 2% (i.e., the difference between the total cell area under coverage and the splat area). For every incoming droplet, the program calculated the resulting splat thickness and the expected diameter based upon the spread factor when the particle was impacting normally to the substrate (zero inclination angle). However, when particle was impacting at an inclined angle, the expected lengths along the major and minor axes of the ellipse were calculated by the aspect ratio by looking up the equation. The program worked out the number of cells to be covered by the splat at the locality of the impact. The procedures were iterated for all the impacting particles. The splat thicknesses were accumulated at the overlapping region to finally build up the deposit.

4.1 Modeling Assumptions for SCM

The SCM was based on the following assumptions:

1. It was assumed that molten particles formed perfect circular discs upon impacting the substrate without any splashing phenomenon or breakup in the case of impact at normal to the substrate. For oblique impact, the resultant splat was assumed to be elliptical in shape. Both assumptions are supported by the SEM micrographs of the splats shown in Fig. 3.
2. Although it accounts for 10-30% of the total volume of the deposit, porosity was neglected in the simplified model. From the published literature, there are different possible sources of porosity, such as peripheral curl up of individual splats, overflowing of liquid over solidified splat, presence of unmelted particles, incomplete filling of the interstices, entrapment of gas between splats, etc. The first effect had been studied extensively by Ghafouri-Azar et al. (Ref 26 and 27) and Xue et al. (Ref 28). However, for yttria-partially-stabilized (8%) zirconia spraying under the same conditions as this study, other sources may be dominant. Therefore, the origin and nature of porosity deserve further study before developing a model to account for the porosity.
3. From the work by Wan et al. (Ref 29), it is noted that for the typical process values of droplet diameter and velocity ranges, all the zirconia droplets were in the viscous dissipation dominant region, implying that the surface tension and wettability effects could be ignored. However, the effects of surface tension and wettability were captured in this model by the experimental measured spread factors and aspect ratios.
4. Table 1 shows the experimental spread factors for zirconia particles sprayed at different operating conditions on a wide range of substrate materials (glass, stainless steel, and steel precoated with zirconia) and surface roughness (Ra values range from 0.02 to 9 μm). Despite the wide ranging process conditions, the variation of spread factors is not significant when considered together with the presence of experimental scatter. Thus, the substrate was assumed to be smooth and the spread factor for zirconia droplet spreading on previously coated zirconia layer was assumed the same as zirconia on smooth steel substrate.
5. Not all particles emitting from the plasma torch would form splats due to particle losses through vaporization, overspray, and rebound at the substrate, the latter two effects are more severe at high-inclination angles. To take into account of particle losses in the simulation, the total number of incident particles was reduced by the experimentally derived Deposition

Efficiency (DE) of the process. This was measured by spraying 50×50×3 mm (thickness) substrates for 5 s and weighing the substrate before and after spraying. The ratio of the weight of deposit (i.e., the difference in weight of substrate before and after spraying) to the weight of powder injected during the same time duration gave the resulting DE. In this experiment, the spraying conditions are given in Table 2 and the resulting DE with increasing of inclination angles is shown in Fig. 6.

Table 2 Experimental spraying conditions

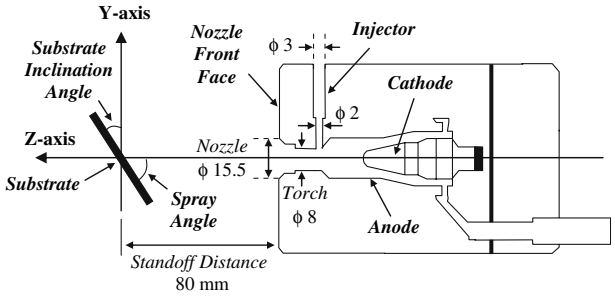

Parameter, unit	Magnitude
Powder size, μm	22-125
Nozzle diameter, mm	15.5
Torch diameter, mm	8
Injector diameter, mm	2
Injector location	Internal
Current, A	900
Voltage, V	35
Primary gas flow rate (Argon), psi (slm)	80 (72)
Carrier gas flow rate (Argon), psi (slm)	30 (4.2)
Powder feedrate, g/min	9.6
Standoff distance, mm	80

4.2 Modeling of Single Splat for Perpendicular and Oblique Impacts

A single spherical droplet, with incident temperature (T_p), velocity (u_p) and diameter (D_p), transforms into a circular splat with diameter, d during perpendicular impact as seen in Fig. 7(a). For the case of droplet impacting at an inclination angle, an elliptical splat with major diameter, d_y and minor diameter, d_x, is obtained as shown in Fig. 7(b). For different impacting angles, the impact site is also different with respect to the splat. For a circular splat, the impact site is at the center of the splat while for the oblique impact which would result in an elliptical shaped splat, the impact site is located at approximately near one of the foci of the ellipse.

At each impact location, the equivalent diameter, d_e was calculated from Eq 5:

$$d_e = \xi D_p \quad \text{(Eq 5)}$$

The particle diameter, D_p was known from the spatial distribution of particle in-flight parameters obtained by CFD simulation as shown in Fig. 2(a) and the spread factor, ξ could be obtained from best-fitted Eq 3.

In the case of perpendicular impact, the splat diameter, d equaled to the equivalent diameter. For oblique impact, it was necessary to convert the equivalent splat of circular shape to an elliptical splat having the same area by reshaping it with the aspect ratio, ψ. The aspect ratio was empirically obtained as a best-fitted Eq 4.

The transformation of a circular splat of the equivalent diameter to an elongated splat was based upon conservation of volume. For same splat thickness, the areas were equivalent.

Area of ellipse = Area of equivalent splat of circular shape

$$\pi \frac{d_x}{2}\frac{d_y}{2} = \frac{\pi d_e^2}{4}$$

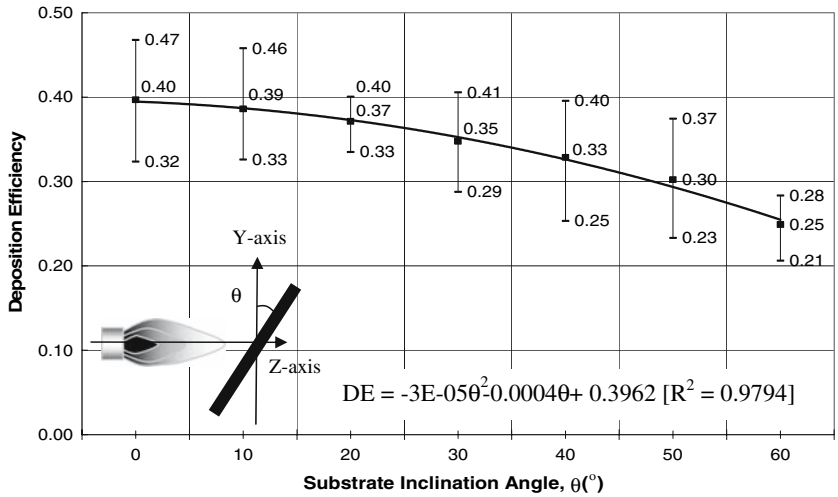

Fig. 6 Deposition efficiencies for different inclination angles

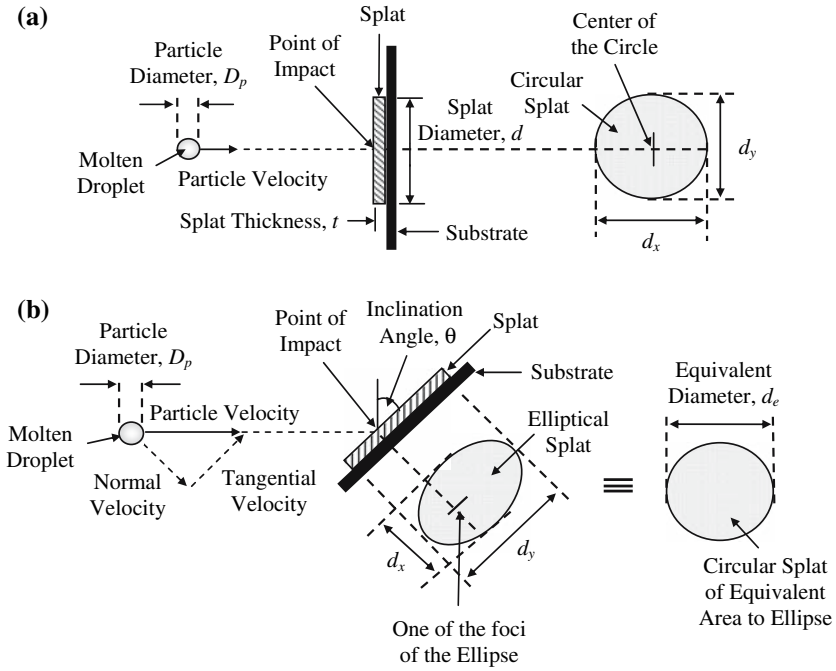

Fig. 7 Idealized illustration of: (a) perpendicular impact of molten particle resulting in circular splat with diameter, d and (b) oblique impact of molten particle resulting in elongated splat with its aspect ratio, ψ of d_y/d_x and its equivalent diameter, d_e

$$d_x d_y = d_e^2 \qquad \text{(Eq 6)}$$

From Eq 2 and 6, the major diameter, d_y and minor diameter, d_x could be computed from the following:

$$d_x = \frac{d_e}{\sqrt{\psi}} \qquad \text{(Eq 7)}$$

Substitute Eq 7 into Eq 6 gave,

$$d_y = d_e\sqrt{\psi} \qquad \text{(Eq 8)}$$

Thus, the dimensions of the elliptical splat were known.

The circular splat with diameter, d and elliptical splat with major diameter, d_y and minor diameter, d_x were then formed on the matrix of discretized 8 μm×8 μm cells as seen in Fig. 8(a) and (b), respectively.

In order to determine which cells in the matrix should be assigned the splat thickness, the root locus of ellipse, r was calculated from Eq 9:

$$\text{The root locus for ellipse, } r = \left(\frac{x}{d_x/2}\right)^2 + \left(\frac{y}{d_y/2}\right)^2 \qquad \text{(Eq 9)}$$

Any cell with its centriodal coordinate (x, y) that fall inside the circumscribing circle or ellipse ($r<1$) as depicted schematically in Fig. 8(c) would be considered as part of the splat and assigned a splat thickness t.

The splat thickness, t was derived based on the concept of conservation of volume, that is, the volume of the splat equals the volume of the originating droplet.

Volume of the splat, V_s = Volume of the droplet, V_p

$$\frac{\pi d_e^2}{4} t = \frac{\pi D_p^3}{6}$$

Therefore, the thickness of the splat was,

$$t = \frac{2D_p^3}{3d_e^2} \qquad \text{(Eq 10)}$$

or in terms of spread factor:

$$t = \frac{2D_p}{3\xi^2}. \qquad \text{(Eq 11)}$$

4.3 Modeling of Multiple Overlapping Splats

In reality, there are large numbers of particles and this leads to the splats overlapping which have to be taken into account. Figure 9 schematically shows the concept of two splats overlapping initially. At the overlap region, simple addition of their individual splat thicknesses was carried out. Based on this concept, the process of accumulating the thickness was repeated for all the incoming particles. The cumulative effect finally yielded the coated deposit.

5. Brief Description on Deposition Experiment Procedure

In order to verify the calculated deposit profiles, experiments were conducted under the same conditions as the numerical simulation conditions. Deposits were

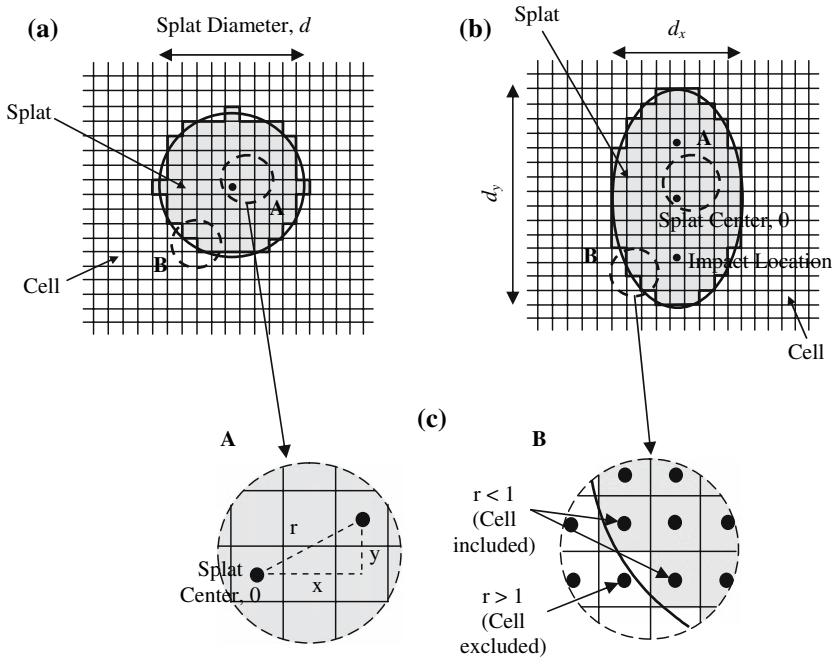

Fig. 8 (a) Circular splat and (b) elliptical splat where the cells shaded in gray are covered by the splat. (c) Enlarged view of regions *A* and *B* denoted by *A* and *B* illustrating cells inclusion processing at the boundary for splat thickness calculation

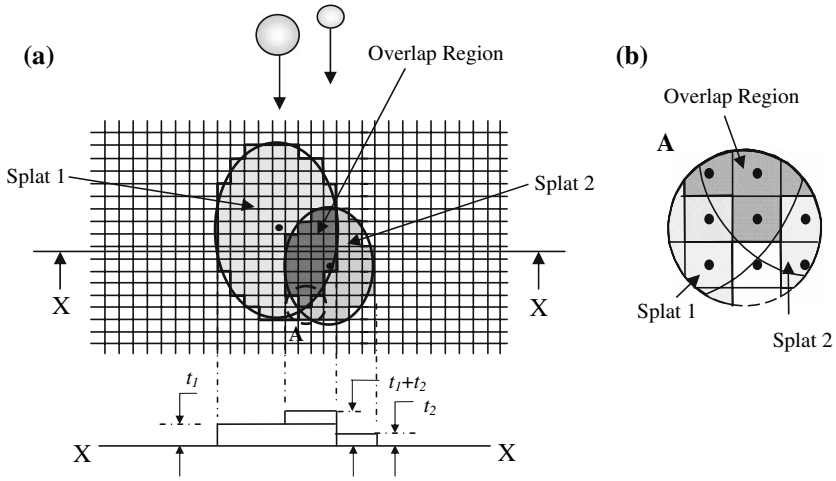

Fig. 9 (a) Schematic illustration depicting the thickness buildup of two overlapping elliptical splats. Each cell records the accumulated height of splats that happen to overlay above it, as seen by sectional view through section *X-X* and (b) shows the enlarged view *A* at the overlap region

sprayed at stationary substrates under different substrate inclination angles. First, substrates were cut and grit-blasted to obtain sufficiently rough surfaces for the deposits to adhere.

The experiment setup is shown in Fig. 10. A movable cover plate was manually placed between the spray torch and the target substrate before the spray system was switched on. After the spray system was operating in a steady state, the cover plate was lifted momentarily to expose the substrate to the spray particles for timed duration of 5 s. Subsequently, the cover plate was dropped to block off the spray particles. The deposits obtained at the different inclination angles were measured by a high-precision metrology Coordinate Measurement Machine (CMM) system 'MahrVision OMS 400©' (Mahr Federal Inc., 1144 Eddy Street, P.O. Box 9400, Providence, RI 02940). The CMM is a non-contact laser measurement system which provides point-to-point three-dimensional

surface height to a resolution of 1 μm. The measurements were then post-processed by digital plotting software Surfer V8.01© (Golden Software Inc., 809 14th Street Golden, CO 80401-1866) to obtain the deposit volumes and thicknesses. For each inclination, three test runs were conducted and a total of 21 substrates were sprayed for 0° to 60° in steps of 10°.

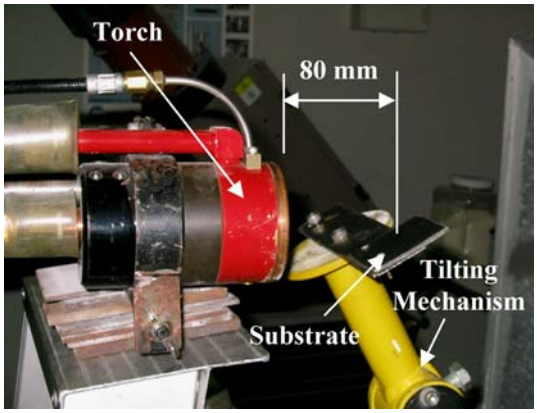

Fig. 10 Setup for thermal-sprayed deposit experiment, with 50° inclined substrate at a standoff distance of 80 mm in front of spray nozzle

6. Results and Discussion

Comparisons of deposit volume and thickness between computed results and experimentally obtained deposits are discussed in the next section.

6.1 Computed and Experimentally Derived Deposits

Figures 11(a)-13(a) show SCM predictions of the three-dimensional coating profiles for substrates inclined at 0°, 30°, and 60° after a spray duration of 5 s. The experimentally obtained deposits sprayed under the same conditions and later measured by a laser-based Coordinate Measurement Machine (CMM) are shown in Fig. 11(b)-13(b).

The good agreement between the predicted and the experimentally measured deposit profiles based on both the peak thickness and widths in X and Y directions indicates that the concept of the SCM is feasible.

6.2 Comparison of Deposit Volumes obtained at Different Substrate Inclinations

Figure 14 shows the comparison of deposit volumes gained by means of experimental spraying and simulation. The experimentally sprayed deposit was scanned by laser

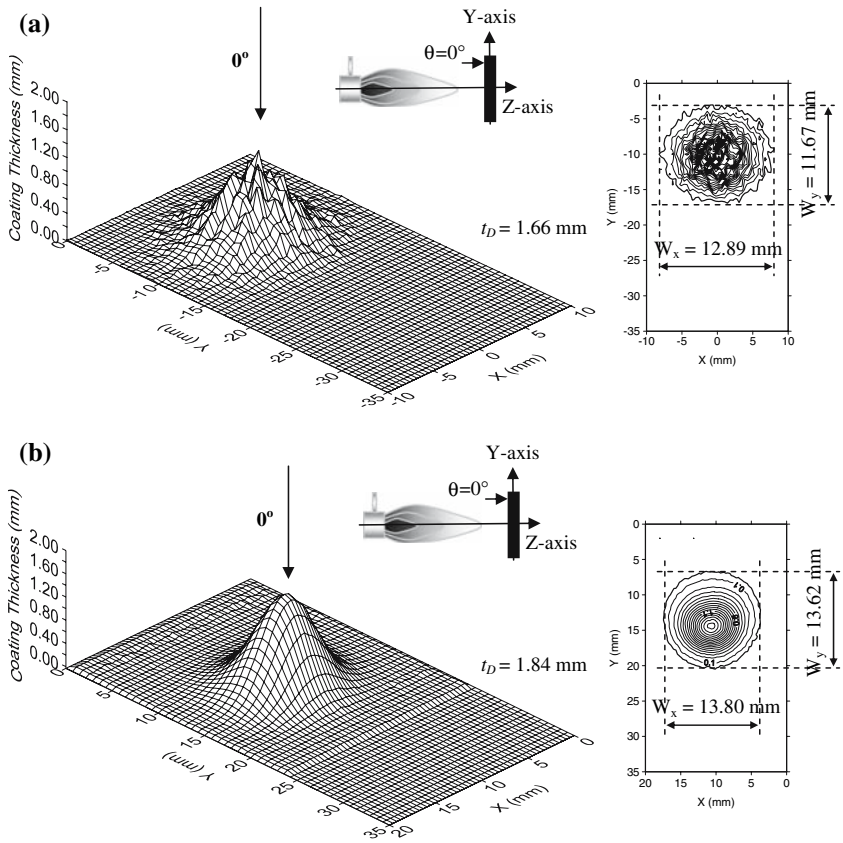

Fig. 11 (a) Computed deposit profile and (b) experimentally obtained deposit of 0° substrate inclination angle showing the three-dimensional deposits (left) and illustrating the deposit contours (right). Arrows indicate the direction of incoming particles

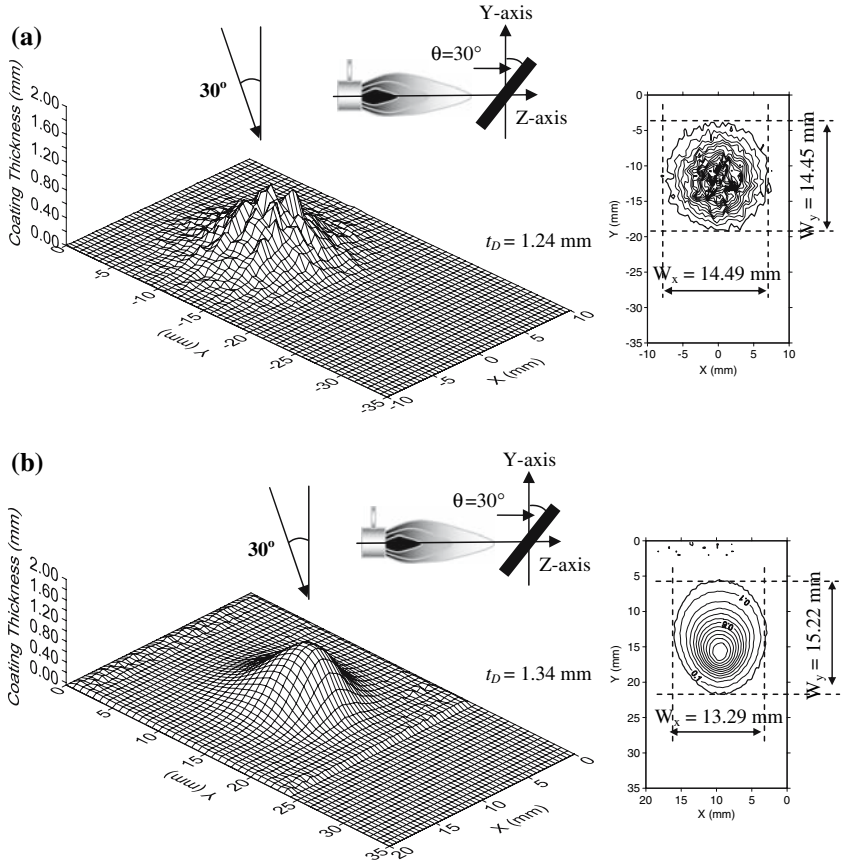

Fig. 12 Similar to layout in Fig. 11 for 30° substrate inclination angle

Coordinate Measurement Machine (CMM) to measure the height profile which was subsequently integrated to yield the total volume of the deposit. The volume obtained thus includes any porosity inherent in the deposit. The computed (simulated) volumes which did not model the porosity formation are slightly lower compared to the experimentally obtained volumes. The difference in volumes between the two methods is the amount of porosity inherent in the deposit. The percentage of porosity can be estimated from Eq 12:

$$\text{Porosity}(\%) = 100 \times \left[\frac{(\text{Scanned} - \text{Computed})\,\text{Deposit volume}}{\text{Scanned deposit volume}}\right] \quad \text{(Eq 12)}$$

In Fig. 14, an increasing trend of porosity with substrate inclination angle is noted. The increase in porosity is partly due to the change of particle impacting momentum with substrate inclination angle. When impacting at higher substrate inclination angle, the particle momentum in the normal direction (i.e., perpendicular to the substrate surface) is reduced in exchange with its tangential component (i.e., parallel to the substrate surface). Particle with lower normal momentum component does not have sufficient energy to adhere and thus will not effectively cover the roughened surface of the substrate or previously deposited splats, i.e., lower normal momentum component of molten particle produces a porous deposit. The same trend was also found in Leigh and Berndt (Ref 30), who reported the increase of porosity from 2.1 to 4.5% for Cr_3C_2-NiCr and from 2.5 to 4.2% for NiAl when the substrate inclination increased from 0° to 40°. The quantitative discrepancy is due to the different types of spray powder used. In their study, metallic powders were sprayed. Metallic powder has lower melting point and lower viscosity at higher temperature compared to the ceramic powder, thus is easily melted, spreads and adheres on the substrate or previously deposited layers thereby resulting in a denser deposit.

For quantitative substantiation, the predicted porosity for perpendicular impact was compared to that measured experimentally by Friis et al. (Ref 31). In their study, the same material as this work, i.e., yttria-stabilized zirconia was sprayed perpendicularly on a substrate to produce thermal barrier coating. The total porosity of the coating which was the sum of all voids, i.e., small pores, large pores, delaminations, and small vertical cracks was determined by two methods, i.e., image analysis and water immersion. The image analysis was conducted on the photographs acquired with scanning electron microscope (SEM) while the water immersion method based on

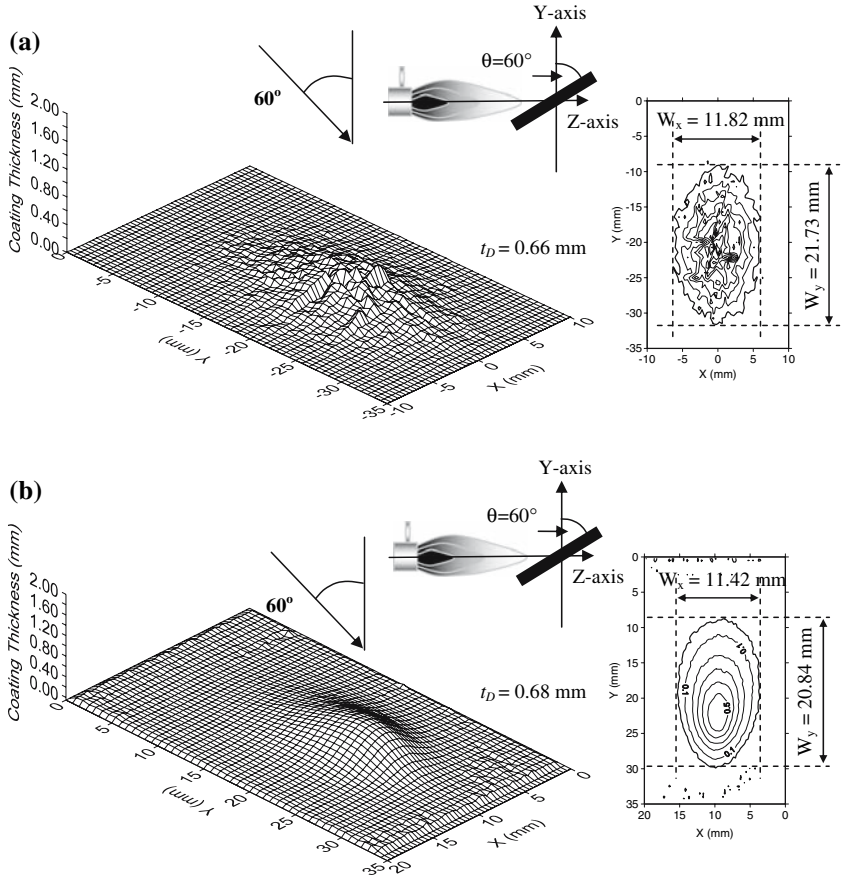

Fig. 13 Similar to layout in Fig. 11 for 60° substrate inclination angle

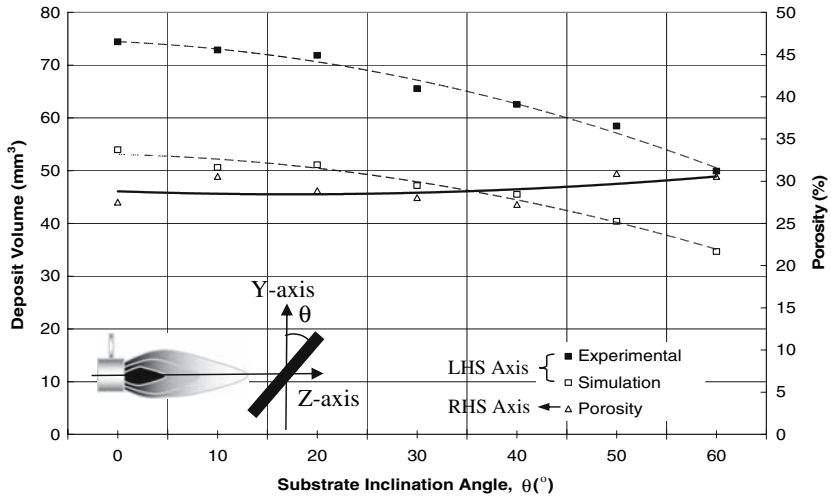

Fig. 14 Deposit volumes gained from experiment by CMM scanning (■) and simulation (□) after 5 s stationary spraying at different substrate inclinations. Deposit porosity is estimated from the difference in the deposit volumes

Archimedes principle. The results showed that the total porosity ranged from 15 to 23%, while in this work, the predicted porosity is 27%.

In addition, Fig. 14 clearly indicates the reducing trends of scanned and computed deposit volumes with increasing substrate inclinations. The main reason is that at lower glancing angle (or higher substrate inclination angle); particles are more likely to be deflected away from the substrate, resulting in lower deposition efficiency.

Table 3 Comparison of the computed and experimentally obtained deposit thicknesses for 0° to 60° substrate inclinations in terms of percentage difference

	Deposit thickness, t_D measured at the peak, mm		
Substrate inclination angle (°)	Computed from SCM	Experiment	Percentage difference[a], %
0	1.66	1.84 (2.03-1.63)	9.63
10	1.55	1.84 (2.17-1.45)	15.92
20	1.48	1.69 (1.90-1.48)	12.63
30	1.24	1.34 (1.43-1.20)	7.45
40	1.02	1.09 (1.12-1.03)	5.97
50	0.79	0.93 (0.98-0.89)	14.72
60	0.66	0.68 (0.75-0.59)	2.77

[a]Note: Percentage difference = 100 × [ABS (Experiment − Simulation)/Experiment].
Values in brackets indicate the ranges of experimentally measured deposit thicknesses.

6.3 Deposit Thicknesses at Different Substrate Inclinations

Table 3 lists the quantitative comparison of the computed deposit thicknesses with experimentally measured peak thicknesses for all substrate inclinations. The maximum deposit thickness occurs at 0° substrate inclination in both cases, with computed value of 1.66 mm and experimental value of 1.84 mm. The deposit thicknesses decrease to minimum values of 0.66 and 0.68 mm for simulation and experiment, respectively, both for 60° substrate inclination. From Table 3, a maximum percentage difference of 16% is observed at 10° inclination. At 60°, the SCM predicts the closest value of deposit thickness to the experiment, with only 3% percentage difference. This shows that SCM also provides fairly good prediction for the deposit thickness.

As a further observation from Table 3, it is noted that there is a reducing trend of deposit peak thicknesses with increasing substrate inclination angles. This is because the deposit thickness is a reflection of the deposition efficiency, i.e., the lower the deposition efficiency, the lower the value of the deposit thickness. In addition, at higher substrate inclination angle, particle plume diverges and covers larger sprayed area and therefore, the particle concentration is widely dispersed. Consequently, the maximum deposit thickness decreases with substrate inclination angle.

Deposits obtained from the SCM have been compared with those obtained from the experiment. The model is capable of predicting the behavioral trends of deposit characteristics; i.e., decrease of deposit volume and thickness as the substrate inclination angle increases.

7. Conclusions

The SCM was developed for the prediction of deposits at different substrate inclinations. This was a semi-empirical model that combined experimentally measured spread factors and aspect ratios with particle dispersion data derived from CFD analysis. The computed deposits when compared with experimental measurements under same spraying conditions showed reasonable to good agreement. While the trend in the volume of the experimental deposits agreed well with the computed, they are consistently higher than the computed; the difference is being attributed to significant porosity present in the experimental deposits. One factor which needs to be looked at is the inclusion of porosity in future work. Accounting for the porosity would significantly improve the agreement between the computational and experimental results.

Acknowledgments

The authors would like to acknowledge both the research funding and the scholarship for the first author CW Kang by Nanyang Technological University, Singapore.

References

1. F. Alonso, I. Fagoaga, and P. Oregui, Erosion Protection of Carbon-Epoxy Composites by Plasma-Sprayed Coatings, *Surf. Coat. Tech.*, 1991, **49**, p 482-488
2. E. Çelik, İ.A. Sengil, and E. Avcı, Effect of Some Parameters on Corrosion Behaviour of Plasma-Sprayed Coatings, *Surf. Coat. Tech.*, 1997, **97**, p 355-360
3. E. Çelik, A.S. Demirkıran, and E. Avcı, Effect of Grit Blasting of Substrate on the Corrosion Behaviour of Plasma-Sprayed Al_2O_3 Coatings, *Surf. Coat. Tech.*, 1999, **116-119**, p 1061-1064
4. B. Uyulgan, H. Cetinel, I. Ozdemir, C. Tekmen, S.C. Okumus, and E. Çelik, Friction and Wear Properties of Mo Coatings on Cast-iron Substrates, *Surf. Coat. Tech.*, 2003, **174-175**, p 1082-1088
5. I. Ozdemir, C. Tekmen, S.C. Okumus, and E. Çelik, Thermal Behaviour of Plasma-Sprayed Mo Coating on Cast-iron Substrate, *Surf. Coat. Tech.*, 2003, **173-174**, p 1064-1069
6. E. Tzimas, H. Müllejans, S.D. Peteves, J. Bressers, and W. Stamm, Failure of Thermal Barrier Coating Systems under Cyclic Thermomechanical Loading, *Acta Mater.*, 2000, **48**, p 4699-4707
7. F.I. Trifa, G. Montavon, and C. Coddet, On the Relationships between the Geometric Processing Parameters of APS and the Al_2O_3–TiO_3 Deposit Shapes, *Surf. Coat. Tech.*, 2005, **195**, p 54-69
8. F.I. Trifa, G. Montavon, C. Coddet, P. Nardin, and M. Abrudeanu, Geometrical Features of Plasma-Sprayed Deposits and Their Characterization Methods, *Mater. Charact.*, 2005, **54**, p 157-175
9. K. Remesh, S.C.M. Yu, H.W. Ng, and C.C. Berndt, Computational Study and Experimental Comparison of the In-flight Particle Behavior for an External Injection Plasma Spray Process, *J. Therm. Spray Technol.*, 2003, **12**(4), p 508-522

10. J.P. Delplanque and R.H. Rangel, A Comparison of Models, Numerical Simulation and Experimental Results in Droplet Deposition Processes, *Acta Mater.*, 1998, **46**(14), p 4925-4933
11. B. Liu, T. Zhang, and D.T. Gawne, Computational Analysis of the Influence of Process Parameters on the Flow Field of Plasma Jet, *Surf. Coat. Tech.*, 2000, **132**, p 202-216
12. T. Zhang, D.T. Gawne, and B. Liu, Computer Modeling of the Influence of Process Parameters on the Heating and Acceleration of Particles during Plasma Spraying, *Surf. Coat. Tech.*, 2000, **132**, p 233-243
13. C.H. Chang and J.D. Ramshaw, Numerical Simulations of Argon Plasma Jets Flowing into Cold Air, *Plasma Chem. Plasma P.*, 1993, **13**(2), p 189-209
14. G. Trapaga and J. Szekely, Mathematical Modeling of the Isothermal Impingement of Liquid Droplets in Spraying Processes, *Metall. Mater. Trans. B*, 1991, **22**, p 901-914
15. Z.G. Feng, G. Montavon, Z.Q. Feng, C. Coddet, and M. Domaszewski, Finite Element Modeling of Liquid Particle Impacting onto Flat Substrates, *Proc. of the 15th International Thermal Spray Conference*, Nice, France, 1998, p 395-400
16. H. Zhang, X.Y. Wang, L.L. Zheng, and X.Y. Jiang, Studies of Splat Morphology and Rapid Solidification during Thermal Spraying, *Int. J. Heat Mass Tran.*, 2001, **44**, p 4579-4592
17. M. Pasandideh-Fard, V. Pershin, S. Chandra, and J. Mostaghimi, Splat Shapes in a Thermal Spray Coating Process: Simulations and Experiments, *J. Therm. Spray Technol.*, 2002, **11**(2), p 206-217
18. J. Mostaghimi, M. Pasandideh-Fard, and S. Chandra, Dynamics of Splat Formation in Plasma Spray Coating Process, *Plasma Chem. Plasma P.*, 2002, **22**(1), p 59-84
19. H. Liu, E.J. Lavernia, and R.H. Rangel, Numerical Simulation of Impingement of Molten Ti, Ni and W Droplets on a Flat Substrate, *J. Therm. Spray Technol.*, 1993, **2**(4), p 369-378
20. M. Bussmann, S. Chandra, and J. Mostaghimi, Numerical Results of Off-angle Thermal Spray Particle Impact, *Proc. of UTSC'99*, Düsseldorf, Germany, 1999, p 17-19
21. R. Ghafouri-Azar, J. Mostaghimi, and S. Chandra, Deposition Model of Thermal Spray Coatings, *Thermal Spray 2001: New Surfaces for a New Millennium*, Ohio, USA, 2001, p 951-958
22. C.W. Kang and H.W. Ng, Splat Morphology and Spreading Behavior due to Oblique Impact of Droplets onto Substrates in Plasma Spray Coating Process, *Surf. Coat. Tech.*, 2006, **200**, p 5462-5477
23. A.C. Leger, M. Vardelle, A. Vardelle, B. Dussoubs, and P. Fauchais, Splat Formation: Ceramic Particles on Ceramic Substrate. *Thermal Spray Science and Technology, ASM International*, Ohio, USA, 1995, pp 169-174
24. M. Vardelle, P. Fauchais, A. Vardelle, and A.C. Leger, Influence of the Variation of Plasma Torch Parameters on Particle Melting and Solidification, *Thermal Spray: A United Forum for Scientific and Technological Advances, ASM International*, Ohio, USA, 1997, p 535-541
25. A. Kucuk, R.S. Lima, and C.C. Berndt, Influence of Plasma Spray Parameters on Formation and Morphology of ZrO_2-8wt% Y_2O_3 Deposits, *J. Am. Ceram. Soc.*, 2001, **84**(4), p 693-700
26. R. Ghafouri-Azar, J. Mostaghimi, S. Chandra, and M. Charmchi, A Stochastic Model to Simulate the Formation of a Thermal Spray Coating, *J. Therm. Spray Technol.*, 2003, **12**, p 53-69
27. R. Ghafouri-Azar, J. Mostaghimi, and S. Chandra, Modeling Development of Residual Stresses in Thermal Spray Coatings, *Comp. Mater. Sci.*, 2006, **35**, p 13-26
28. M. Xue, J. Mostaghimi, and S. Chandra, Investigation of Splat Curling up in Thermal Spray Coatings, *Proceedings of the International Thermal Spray Conference*, Seattle, WA, USA, 2006
29. Y.P. Wan, H. Zhang, X.Y. Jiang, S. Sampath, and V. Prasad, Role of Solidification, Substrate Temperature and Reynolds Number on Droplet Spreading in Thermal Spray Deposition: Measurements and Modeling, *J. Heat Trans.-T. ASME*, 2001, **123**, p 382-389
30. S.H. Leigh and C.C. Berndt, Evaluation of Off-angle Thermal Spray, *Surf. Coat. Tech.*, 1997, **89**, p 213-224
31. M. Friis, C. Persson, and J. Wigren, Influence of Particle In-flight Characteristics on the Microstructure of Atmospheric Plasma Sprayed Yttria Stabilized ZrO_2, *Surf. Coat. Tech.*, 2001, **141**, p 115-127